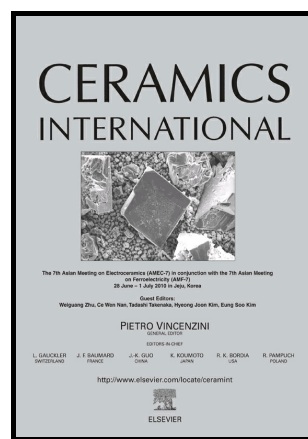


Molecular Dynamics Simulation of Silicon Carbide
Nanoscale Material Removal Behavior

Yao Liu, Beizhi Li, Lingfei Kong



www.elsevier.com/locate/ceri

PII: S0272-8842(18)30761-2
DOI: <https://doi.org/10.1016/j.ceramint.2018.03.195>
Reference: CER117832

To appear in: *Ceramics International*

Received date: 5 March 2018
Revised date: 21 March 2018
Accepted date: 21 March 2018

Cite this article as: Yao Liu, Beizhi Li and Lingfei Kong, Molecular Dynamics Simulation of Silicon Carbide Nanoscale Material Removal Behavior, *Ceramics International*, <https://doi.org/10.1016/j.ceramint.2018.03.195>

This is a PDF file of an unedited manuscript that has been accepted for publication. As a service to our customers we are providing this early version of the manuscript. The manuscript will undergo copyediting, typesetting, and review of the resulting galley proof before it is published in its final citable form. Please note that during the production process errors may be discovered which could affect the content, and all legal disclaimers that apply to the journal pertain.

Molecular Dynamics Simulation of Silicon Carbide Nanoscale Material Removal Behavior

Yao Liu^{1,2}, Beizhi Li^{1,2,*}, Lingfei Kong²

Department of Mechanical Engineering, Donghua University, Shanghai 201620, China

Department of Mechanical Engineering, University of Michigan, Ann Arbor, MI 48105, USA

**Corresponding author: lbzhidhu@163.com*

Abstract

The scratching processes of monocrystalline and polycrystalline silicon carbide (SiC) with diamond grit were studied by molecular dynamics simulation to investigate the material removal behavior in this study. The results showed that, for both monocrystalline and polycrystalline SiC, the material removal process was achieved by the phase transition to the amorphous structure. Large depth of cut and low scratching speed induced the large scratching forces, stress, and surface damage layer thickness. Less amorphous structure phase transition, smaller normal scratching force, and higher tangential stress were found in polycrystalline SiC, comparing the monocrystalline SiC, due to the material soften caused by the microstructure in all scratching conditions. Furthermore, the tangential stress showed highly dependent on the grain geometry and grain boundary (GB) location in polycrystalline. The subsurface damage layer in polycrystalline was little thinner than that in monocrystalline before the new GB generation at a low depth of cut and deteriorated at large depth of cut. In addition to the plastic deformation, which occurred in the monocrystalline SiC nanoscale scratching, the intergranular fracture and transgranular fracture were also observed through the GB generation and connection in polycrystalline SiC.

Keywords: Crystal structure; Deformation and fracture; Grain boundary; Microstructure; Phase transformation

1. Introduction

Silicon carbide (SiC) is a promising material for space telescope mirror and large-scale ground reflectors due to the extremely high stiffness, high thermal conductivity, and outstanding dimensional stability [1]. However, high hardness and low fracture toughness make SiC machining inefficient and high cost. For the low-cost machining and rapid delivery of SiC, the understanding of SiC nanoscale scratching behavior is necessary. Molecular dynamics (MD) simulation, which can provide an atomic vision to nanoscale material removal behavior, has been used to investigate the elastic-to-plastic transition [2] and phase transformation [3] in monocrystalline SiC nanoscale machining. However, engineering SiC exists in polycrystalline, formed with many microstructures, such as voids, dislocations, and grain boundaries (GBs), and grain cell, which can affected material strengths [4], fracture toughness [5], plastic deformation mechanism [6], thermal conductive [7], and phase transformation [8]. Different abrasive wear [9], chipping [10], and surface roughness [9,10] have been proved in the polycrystalline and monocrystalline SiC machining experiments. However, no simulation investigation considering the microstructure influences on the SiC scratching behavior had been reported. To bridge the research gap, the nanoscale material removal behaviors of the monocrystalline and polycrystalline SiC were investigated in MD simulation. The material removal process, force, stress, and subsurface damage layer were compared to understand the influences of microstructure.

2. MD model

Fig. 1(a) gives the crystal structures and lattice constants of the diamond grit and SiC ceramic. The potential function for Si-C in SiC is Tersoff, other potential functions are set as Morse. All potential function parameters are from [11]. Figs. 1(b) and (c) gives the monocrystalline and polycrystalline SiC models, which consists of 10 nm diameter diamond grit and cuboid SiC workpiece sized in $30 \times 15 \times 10 \text{ nm}^3$, which was decided by conducting an independent study of workpiece size and scratching force. Totally, 46079 and 438012 atoms were generated in the diamond grit and SiC workpiece, respectively. Three types of atoms: boundary atoms, thermostat atoms, and Newtonian atoms, were defined in the SiC workpiece based on the MD theory. Fig. 1(c) presented the polycrystalline SiC model, which generated by using the modified Voronoi diagrams. Voronoi diagrams [12] used point seeds to divide a region into convex polygons. In this study, the hybrid seeds with rotational matrixes attached on seeds were generated to adjust the region orientation. The Voronoi diagrams with hybrid seeds were used on monocrystalline SiC to generate the grains with different orientation. All grains were assembled to form the polycrystalline SiC workpiece. Other setup in polycrystalline model was same with monocrystalline model.

Totally 18 simulations with 50, 100, and 200 m/s scratching speed and 1, 2, and 3 nm depth of cut were conducted. The scratching distance is 20 nm. All simulations were completed using the LAMMPS with a timestep of 0.001 picoseconds. The scratching process, force, stress, and surface damage layer results were interpreted by the OVITO after the simulation.

3. Results and discussion

Fig. 2 gives material removal and crystal structure evolution in the scratching process. For the monocrystalline SiC, as shown in Fig. 2(a), at 0 nm scratching distance (l), the atoms show the original diamond/zinc blende structure (marked by blue color) except the amorphous atoms (marked by white color) on the surface due to lacking neighbor. As the grit moves to $l=10$ nm, the SiC atoms pile up in the front of grit to generate the deformed chip and flow out to the groove side to generate the protrusion, which makes the atom crystal structure reconstructed and transformed into amorphous. Furthermore, the amorphous structure also shows at grit tip surface of the contact zone due to the silicon atoms penetration, which may cause the wear of the grit. As the grit continues moving, more atoms transfer into amorphous structure. Removing the amorphous structure after 20 nm scratching distance, several atoms in hexagonal diamond structure (orange color) were found due to the phase transition. For the polycrystalline model, presented in Fig. 2(b), the atoms in the GB show the amorphous structure due to disorder structure before the scratching. After the scratching, same phase transition from zinc blende to amorphous and hexagonal diamond structure was discovered. More hexagonal atoms were found accompanied with some dislocation in GBs. Furthermore, new GBs were initialed in the scratching process and connected with the old GBs, which may cause the intergranular removal.

The main material removal process was achieved by the phase transition from zinc blende to amorphous structure in the SiC scratching. The numbers of the hexagonal and amorphous structure atoms were counted before and after scratching. The atoms in hexagonal structure were 0 before scratching and less than 150 after the scratching. The amorphous atom number in monocrystalline increased 11917, 12346, and 12946 at 1 nm depth of cut for 50, 100, and 200 m/s, respectively, indicating the higher scratching speed promotes the more zinc blende structure destruction process due to larger impactation breaking more Si-C bonds. Same trend also found in 2 and 3 nm depth of cut. Compared with monocrystalline SiC, the polycrystalline SiC has less amorphous atom increase, which were 10809, 11196, and 11576 at 1 nm depth of cut for 50, 100,

and 200 m/s. Part of the impaction energy is absorbed by the microstructure which makes the polycrystalline more soften and has less phase transition. This result also indicated that the monocrystalline is more sensitive to the scratching speed and depth of cut.

The forces of monocrystalline and polycrystalline SiC in 200 m/s scratching speed and 3 nm depth of cut is presented in Fig. 3(a). In monocrystalline model, both the tangential and normal forces increase as the grit cuts into the workpiece in 0-5 nm scratching distance. As the scratching distance extends to 5-20 nm, the tangential and normal forces keep stable with few fluctuations, which are caused by the discrete atom position in the nanoscale. The average tangential and normal forces are about 1.9 and 2.8 nN, respectively. The force evolution of polycrystalline SiC shows the similar trend with monocrystalline and the average tangential and normal forces are 1.9 and 2.6 nN, respectively. The similar tangential force in monocrystalline and polycrystalline indicates the minimal effect of microstructure on the material removal energy. However, the normal force is about 9% lower in polycrystalline, which indicates the microstructure makes the SiC softer with lower hardness. Furthermore, a higher normal force variation was found in polycrystalline scratching which was 0.185, comparing to 0.169 in monocrystalline, indicating the inhomogeneous of polycrystalline structure is due to the GBs.

Figs. 3(b) and (c) present the average tangential and normal forces under all scratching speed and depth of cut. With changing of depth of cut and scratching speed, the tangential and normal force of monocrystalline and polycrystalline SiC showed a similar trend, which decreased with the scratching speed due to more defects generation in larger impaction and increased with depth of cut because more material was removed. Under the same scratching parameters, tangential force was same and normal force decreased about 10% in polycrystalline due to the GB soften.

Fig. 4 shows the stress variation with the scratching distance in monocrystalline and polycrystalline SiC. All stresses go through the rapid increase in 0-5 nm scratching speed as the grit cuts into the workpiece. After 5 nm scratching distance, the tangential stress continues increasing and normal stress keeps stable. In monocrystalline, the tangential stress continues increasing from 1.8 to 3.0 GPa in 200 m/s scratching speed and 3 nm depth of cut, presented in Fig. 4(a), due to the defects accumulation. This defects accumulation causes the stress concentration on the material in the front of the grain even in a stable tangential force. The scratching speed effect on the tangential stress is minimal, which is less than 5% in 50-200 m/s. However, in polycrystalline, the tangential stress shows great dependence on the grain geometry

and GB, which can be seen in Fig. 4(b). As the grit engages with different grains, the tangential stress goes through increase with the different slope in the range of 5-9.9, 9.9-14.9, and 17.7-20 nm scratching distance. A slight decrease of the tangential stress is observed when the grit cuts in the 14.9-17.7 nm, which has only one grain engagement. The higher stress in polycrystalline scratching is due to the defects accumulation induced stress concentration. The larger tangential stress deviation in the different scratching stage is caused by different grains size and GBs direction. The scratching speed effect on the tangential stress is also minimal but obviously larger than that in monocrystalline. All the normal stress keeps stable in the range of 5-20 nm scratching speed. The stabilized values in monocrystalline and polycrystalline are 1.6 and 1.7 GPa, which is similar due to same normal force. That trend shows normal stress in polycrystalline is non-sensitive with the grains and GBs, which is also found the other scratching speed and depth of cut.

Table 1 gives the measured subsurface damage (SSD) thicknesses in monocrystalline and polycrystalline SiC at the cross-section view of $Y=7.5$ nm. The SSD thickness is positively correlated with the depth of cut for both monocrystalline and polycrystalline SiC due to more material is removed, which forces more atom structure breakage. Specifically, at 50 m/s scratching speed, the SSD thickness increases from 1.6 to 2.5 and 2.8 nm for the monocrystalline and from 1.0 to 3.9 and 5.1 nm for polycrystalline as the depth of cut increases from 1 to 2 and 3 nm, respectively. Compared the SSD in monocrystalline and polycrystalline, the polycrystalline got a smaller SSD at the 1 nm depth of cut. The softening effect of the GBs makes a smaller SSD in polycrystalline in 1 nm depth of cut, which the plastic deformation dominates the material removal process. A reverse trend with higher SSD in polycrystalline was found at 2 and 3 nm depth of cut, where new GBs generated due to the dislocation extension, transgranular and intergranular fracture, which enlarges the SSD thickness. However, material removal in monocrystalline was also controlled by the plastic deformation. Those results indicate that only the plastic flow exists in the nanoscale monocrystalline SiC, however, for polycrystalline SiC scratching, at least three types of the material removal mechanism - plastic deformation, intergranular fracture, and transgranular fracture - happens due to the existing of microstructure.

4. Conclusions

A methodology to build a polycrystalline MD model with microstructure by using the modified Voronoi diagrams with hybrid seeds was presented. The material removal behaviors of monocrystalline and polycrystalline SiC were compared in nanoscale the scratching. The scratching force, amorphous phase transition, and SSD thickness are increase with the depth of cut and decrease with the scratching speed for both monocrystalline and polycrystalline SiC. The microstructure in polycrystalline makes the SiC more soften by generating less normal scratching force and amorphous structure phase transition and thinner plastic deformation induced SSD. The GB in polycrystalline can be the core for the dislocation generation and extension, which can form new GB, making the nanoscale material removal from the pure plastic deformation in monocrystalline to the hybrid removal with the plastic deformation, intergranular fracture, and transgranular fracture in polycrystalline.

Acknowledgments

This work was supported by the National Natural Science Foundation of China (No. 51675096 and 51475367) and Chinese Universities Scientific Fund (No. CUSF-DH-D-2018087)

References

- [1] Jiang, W, Yang L, Riemer O, Li S, Shen X, Yamamura K, Zhang X, Zhang X, Wang D, Peng K. Research on optimal process parameters in thermally oxidation-assisted polishing of reaction-sintered silicon carbide. AOMATT 2016; 9683:96832B-10.
- [2] Liu Y, Li B, Kong L. Atomistic insights on the nanoscale single grain scratching mechanism of silicon carbide ceramic based on molecular dynamics simulation. AIP Advances 2018; 8:035109. <https://doi.org/10.1063/1.5019683>
- [3] Goel S, Luo X, Comley P, Reuben RL, Cox A. Brittle-ductile transition during diamond turning of single crystal silicon carbide. International Journal of Machine Tools and Manufacture 2013; 65:15-21.
- [4] Shenderova OA, Brenner DW, Omeltchenko A, Su X, Yang LH. Atomistic modeling of the fracture of polycrystalline diamond. Physical Review B 2000; 61(6):3877-3888.

- [5] Latapie A, Farkas D. Molecular dynamics investigation of the fracture behavior of nanocrystalline α -Fe. *Physical Review B*, 2004; 69(13):134110-9
- [6] Li J, Liu B, Luo H. A molecular dynamics investigation into plastic deformation mechanism of nanocrystalline copper for different nanoscratching rates. *Computational Materials Science* 2016; 118:66-76.
- [7] Bagri A, Kim SP, Ruoff RS, Shenoy VB. Thermal transport across twin grain boundaries in polycrystalline graphene from nonequilibrium molecular dynamics simulations. *Nano Lett* 2011; 11(9):3917-21.
- [8] Goel S, Haque FN, Luo X, et al. Nanoindentation of polysilicon and single crystal silicon: Molecular dynamics simulation and experimental validation. *Journal of Physics D: Applied Physics* 2014; 47(27):275304-14.
- [9] Kasuga H, Ohmori H, Mishima T, Watanabe Y, Lin W. Investigation on mirror surface grinding characteristics of SiC materials. *Journal of Ceramic Processing Research* 2009; 10:351-354.
- [10] Cvetković S, Morsbach C, Rissing L. Ultra-precision dicing and wire sawing of silicon carbide (SiC). *Microelectronic Engineering* 2011; 88:2500-2504.
- [11] Liu Y, Li B, Kong L. A Molecular Dynamics Investigation into Nanoscale Scratching Mechanism of Polycrystalline Silicon Carbide Ceramic. *Computational material science* 2018; 148:76-86.
- [12] Voronoï G. Nouvelles applications des paramètres continus à la théorie des formes quadratiques. Deuxième mémoire. Recherches sur les paralléloèdres primitifs. *Journal für die reine und angewandte Mathematik* 1908; 134:198-287.

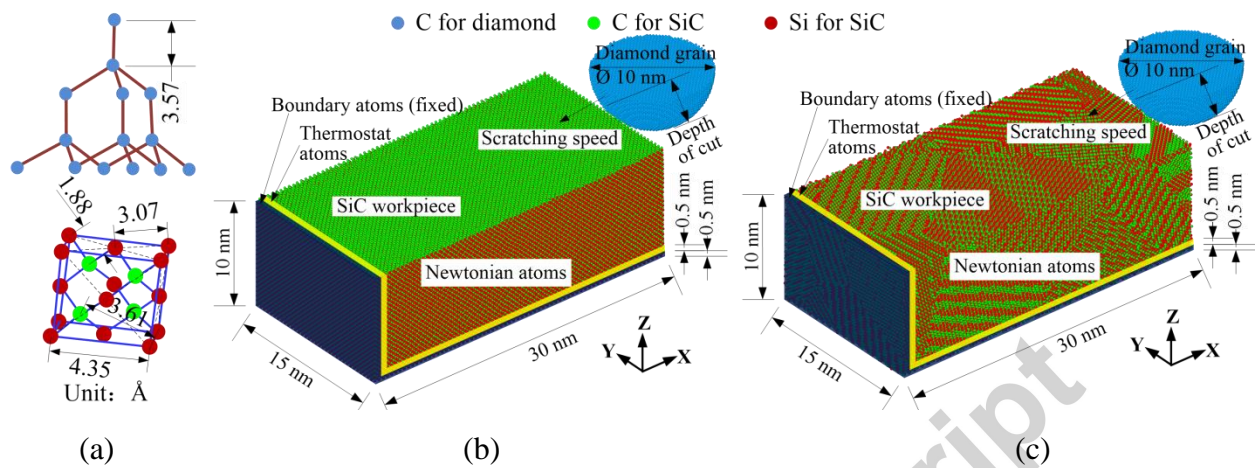


Fig. 1 (a) crystal structure, 3D MD model for (b) monocrystalline and (c) polycrystalline SiC.

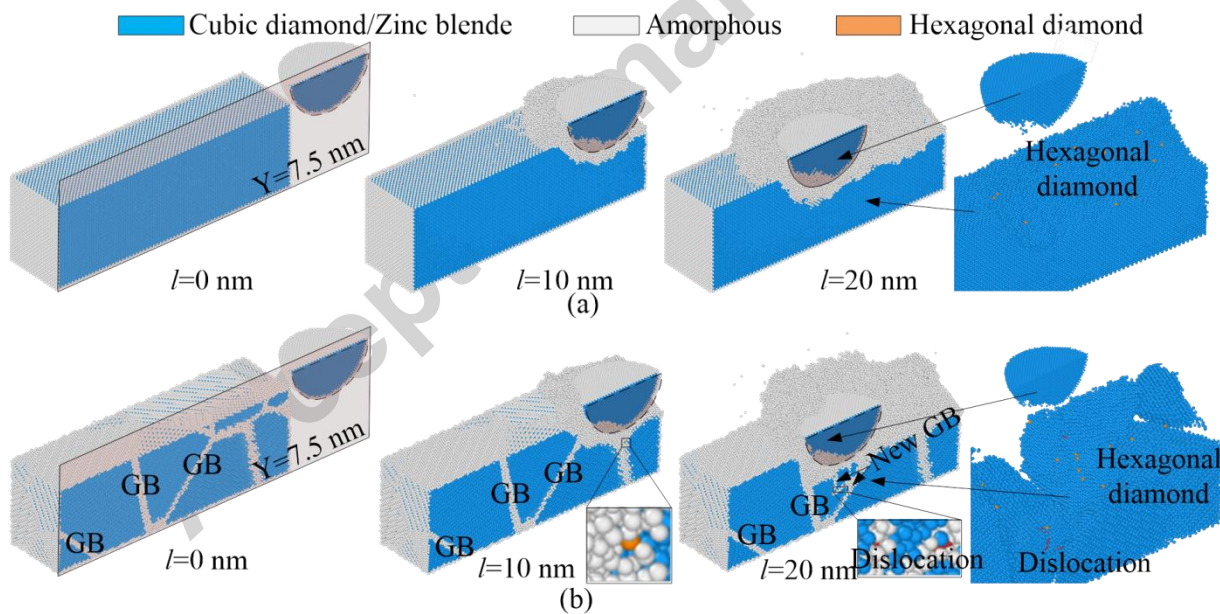


Fig. 2 The crystal structure analysis results at (a) 0, (b) 10, and (c) 20 nm scratching distance.

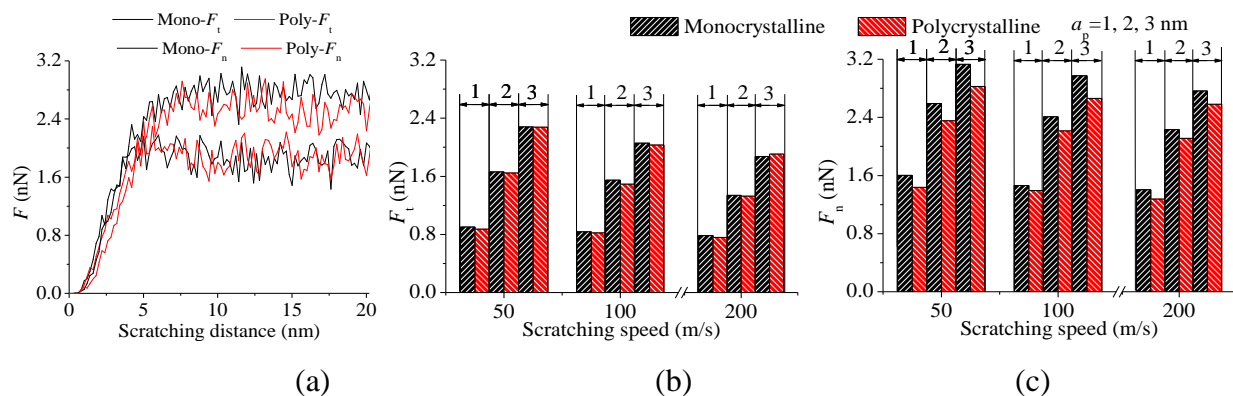


Fig. 3 (a) Scratching force as a function of scratching distance, (b) tangential, and (c) normal force vs. scratching speed under 1, 2, and 3 nm depth of cut.

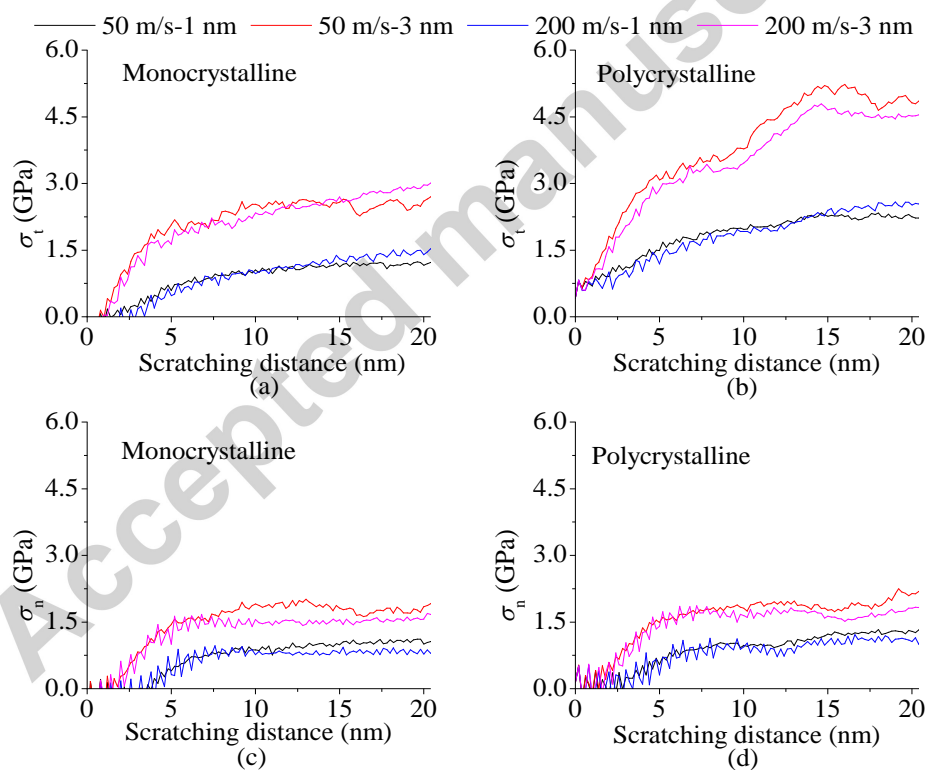
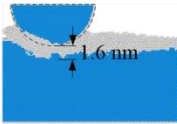
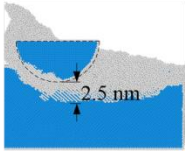
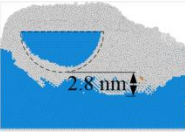
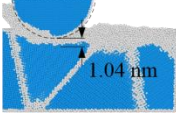
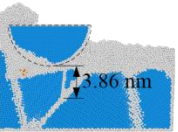
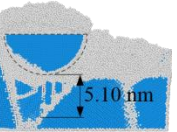
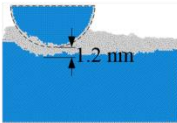
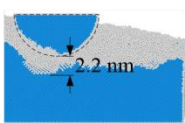
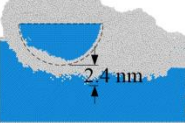
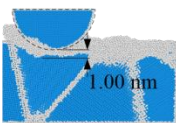
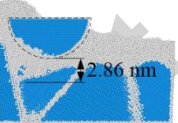
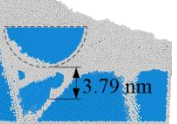


Fig. 4 Stress variation with the grinding distance. (a) Tangential and (b) normal stress.

Table 1 Subsurface damage thickness

Scratching speed	Monocrystalline			Polycrystalline		
	$a_p=1$ nm	$a_p=2$ nm	$a_p=3$ nm	$a_p=1$ nm	$a_p=2$ nm	$a_p=3$ nm
50 m/s						
100 m/s						
200 m/s	